A High-Resolution Vacuum Spectrometer for the Infrared

Tsunetake FUJIYAMA,*1 Jun NAKAGAWA,*2 Isao SUZUKI,*3 Ichiro NAKAGAWA,*4 and Takehiko SHIMANOUCHI

*1 *Department of Chemistry, Faculty of Science, Tokyo Metropolitan University, Setagaya-ku, Tokyo 158*
*2 *Department of Chemistry, Faculty of Science, Hiroshima University, Higashi-Sendamachi, Hiroshima 730*
*3 *Educational Computer Cenret, The University of Tokyo, Bunkyo-ku, Tokyo 113*
*4 *Department of Chemistry, Faculty of Science, Tohoku University, Aoba, Aramaki, Sendai 980*
Department of Chemistry, Faculty of Science, The University of Tokyo, Bunkyo-ku, Tokyo 113

(Received November 20, 1975)

A high-resolution vacuum spectrometer for the near and medium infrared has been designed and built with capability of resolving 0.03 cm^{-1}. The spectrometer consists of the fore-optics with a built-in White cell, a 2.5 m Littrow-McCubbin type monochromator which utilizes a 31.6 lines/mm echelle grating with the ruled area of 102 mm × 206 mm, and an order-sorter which is essentially a prism spectrometer of Wadsworth mount. Details of the design, construction, and performance of the instrument are described.

There are three types of method available for a construction of a high-resolution infrared spectrometer at present. They are dispersion type infrared spectrometer with a large grating, a Michelson type Fourier spectrometer and a spectroscopy using a laser source.

Recently, laser sources have been introduced to infrared spectroscopy and recognized to be very useful sources to obtain magnificient resolution. However, observable spectral regions are confined to the frequency ranges very close to particular laser lines. In order to correlate laser lines to molecular absorption lines, the laser frequencies must be tuned by appropriate methods, *e.g.*, a Zeeman shift technique, or the molecular absorption lines must be moved to the laser frequencies using a Stark effect, a spin-magnetic resonance effect, and so on. These methods can cover very narrow frequency regions, say, ± 1 cm^{-1} from laser frequencies. In the case where a molecule has no dipole moment or electric spin moment, it is impossible to move molecular absorption lines by the above techniques. Although recent developments of dye lasers and semiconductor lasers make it possible to extend the tunable regions considerably, it is not wide enough to use the laser elements in a system for general purposes.

In principle, Fourier spectrometer using Michelson interferometer is the most preferable spectrometer in the respects of a resolution and of observable spectral regions. A resolution which has been actually obtained by the method is about 0.005 cm^{-1} and an observable spectral region 2830—10000 cm^{-1} with a PbS detector.[1] Since a resolution of an interferometer is inversely proportional to a path difference of two interfering beams, one must translate one of the plane mirrors over a long distance with a high accuracy. Suppose the mirror is translated 200 cm, a resolution obtained is 0.005 cm^{-1} so long as an apodization procedure is perfect. During the translation of the mirror, the path differences must be measured with a high accuracy and the direction of the mirror must be kept definitely constant. The other difficulty is a treatment of interferograms. In order to transform an interferogram to a usual spectrum, a computer with large memories must be used, because a number of observed points of a interferogram is numerous.

On the other hand, a large grating high-resolution spectrometer is the most general method and its construction is comparatively easier than the other two methods. Though a resolution obtainable by a large grating spectrometer is much lower than those of the other two methods, this type of spectrometer is more convenient to use than the others in the respect of its construction and its operation. A wide frequency region can be covered by the use of suitable gratings and detectors. Therefore, we decided to construct a large grating spectrometer. Our wishes to study rotational fine structures of vibrational transitions for usual interesting molecules dictated the basic design requirements. Briefly, these were that the instrument should cover the spectral region 600 to 4000 cm^{-1}, that the resolution should be the order of 0.03 cm^{-1} at all wave numbers, that we should be able to handle samples of ordinary interests conveniently, and that the operation and calibration of the instrument should be relatively straightforward. The following items have been mainly taken into account in the design and construction of the present spectrometer, *viz.*,

(1) the resolution is better than 0.04 cm^{-1},

(2) the frequency region covers from 600 to 4000 cm^{-1},

(3) the accuracy of frequency measurement is better than 0.001 cm^{-1},

(4) the accuracy of intensity measurement is better than $\pm 1\%$,

(5) the whole spectrometer system is stable enough to do continuous measurements, and

(6) the lines of atmospheric carbon dioxide and water vapour should be eliminated sufficiently.

A resolution, $\Delta\nu$, of a spectrometer is expressed as

$$\Delta\nu = \frac{d\cdot\cos\theta}{p\cdot n}\cdot\frac{s_1+s_2}{f}\nu^2+\frac{1}{p\cdot 2W\cdot\sin\theta} \qquad (1)$$

where d is a grating constant, p a number of optical paths to the grating, s_1 and s_2 mechanical slit widths of entrance and exit slits, respectively, f a focal length of a collimating mirror, and W a ruled width of the grating. On the other hand, radiant power which arrives at a detector for a particular frequency and a slit width is given by

$$E = \frac{BThAD}{f}\cdot(\Delta\nu)^2 \qquad (2)$$

where B denotes source radiance, T transmittance of a whole spectrometer, h a slit height, A an effective area of a collimating mirror which usually corresponds to a ruled area of a grating, and D angular dispersion of a grating. Equations (1) and (2) show that a resolution is higher as a focal length increases, while energy arrives at a detector decreases as a focal length increases. In order to increase a focal length to realize the required resolution without losing too much energy, an effective area of a collimating mirror, A, and a slit height, h, should be increased at the same time, which leads to the increase of the whole dimensions of a spectrometer.

Most of the large grating spectrometers reported so far have been designed for special uses in the regions above 2800 cm^{-1} and have been used for the observations of the C–H stretching fundamental bands and other summation bands. We referred to the spectrometer constructed in the University of Minnesota,[2] because it satisfies most of the required items for our spectrometer.

Removal of atmospheric carbon dioxide and water vapor was essentially important, because their existence makes it impossible to measure absorption spectra in the regions where these molecules show strong absorption lines, *e.g.*, 2200—2400 cm^{-1} region, 1300—1800 cm^{-1} region, and so on. Therefore a vacuum spectrometer has been considered and the problem of vacuum has been one of the most troublesome problems at all stages in the building.

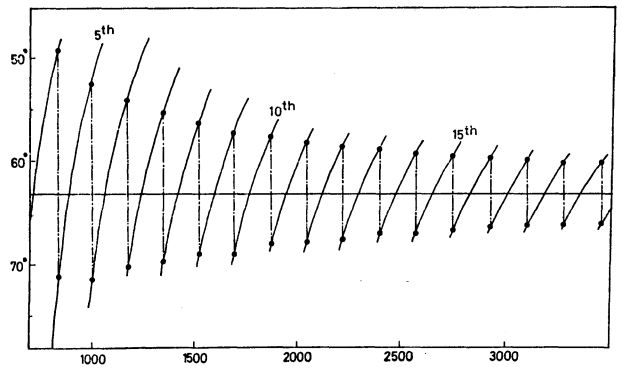

Fig. 1. Relation between angle of incidence on grating and frequency for various grating orders. Actual frequency scanning is performed along the real lines.

A grating is the most important component of an optical system, so we must decide a desirable grating at first to construct the spectrometer. A grating finally chosen is an echelle type plane replica grating made by Bausch and Lomb Co., Ltd. The grating has a ruled area of dimensions 206 mm × 102 mm with 31.6 lines per mm and a blaze angle of 63°26′. This type of grating is superior, in the respect of linear dispersion and brightness, to that of fine echellette, because the latter has a small grating constant, d, and a small blaze angle of about 30°. By the use of the above grating of echelle type, the frequency region of 600—4000 cm^{-1} can be covered by changing a grating order. Figure 1 shows relations between an angle of incidence on the grating and frequencies for various grating orders. The horizontal line corresponds to the blaze angle and, therefore, an actual frequency scanning is performed along the real lines of the figure. It is seen from the figure that the lower a grating order the more angular change is necessary for scanning of the same frequency interval.

Optical Systems

The main part of the monochromator is of Littrow-McCubbin type with an optical system of 2500 mm focal length as shown in Fig. 2. The whole optical system may be classified into three parts, namely, fore-optics with a sampling system, a grating monochromator, and an order sorter.

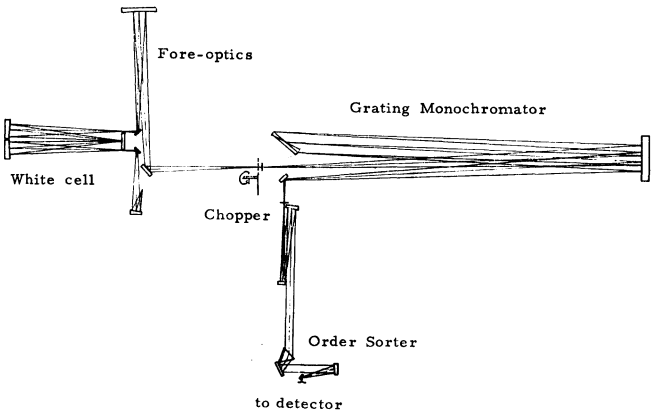

Fig. 2. Optical layout of spectrometer.

Grating Monochromator. A grating monochromator is the most essential of all, because it governs a resolution and an accuracy of frequency measurement. According to Eq. (1), the theoretical resolution for the grating described in the preceding section is 0.027 cm^{-1}

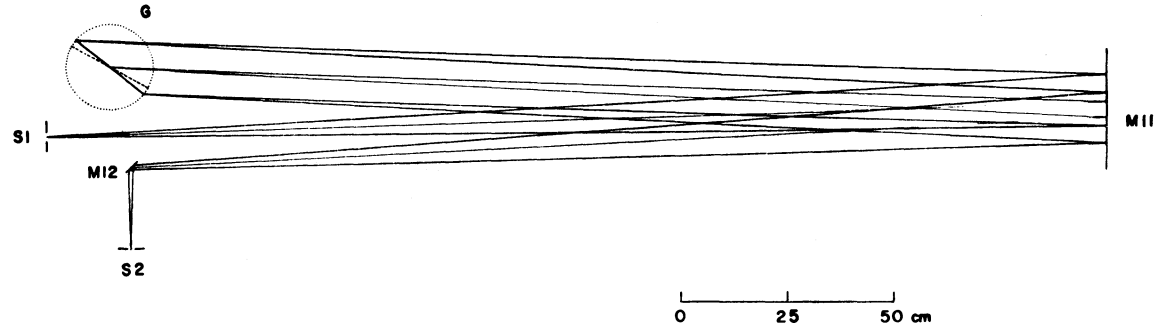

Fig. 3. Optical layout of grating monochromator for single pass operation.

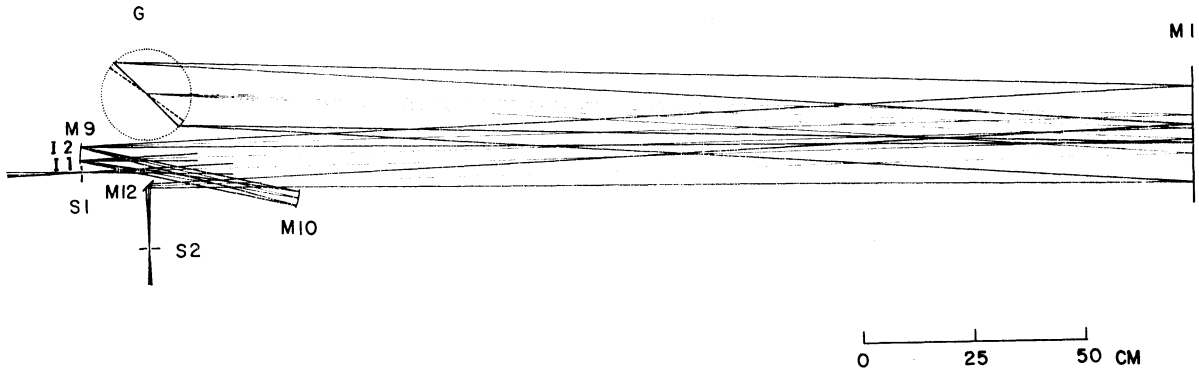

Fig. 4. Optical layout of grating monochromator for double pass operation.

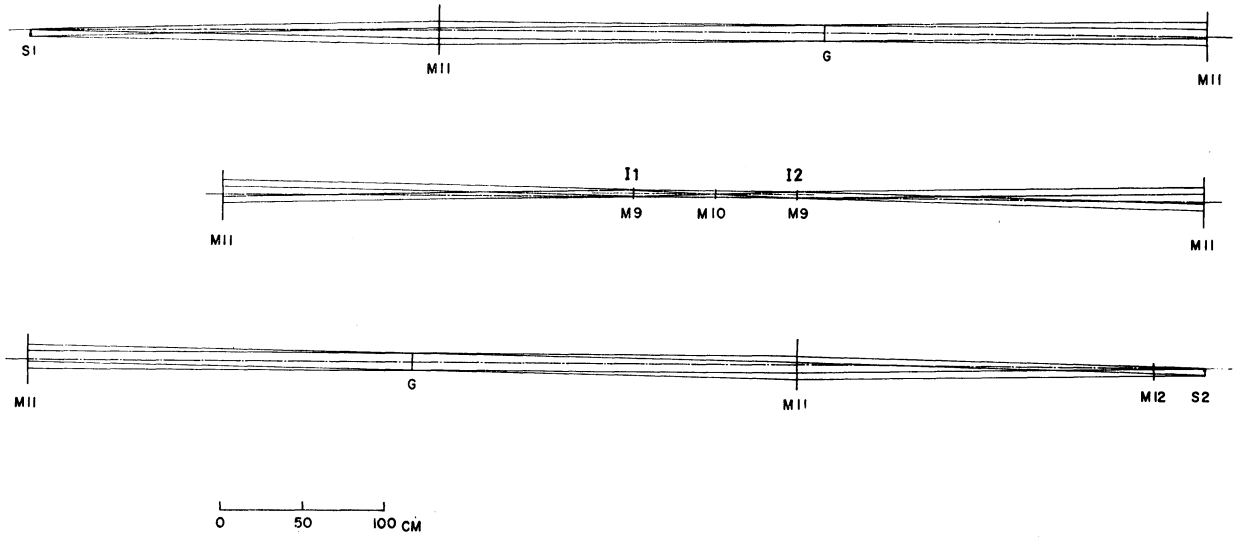

Fig. 5. Vertical tracing of monochromator optics for double pass operation. Single pass component is separated by masking upper halves of entrance and exit slits.

and 0.014 cm^{-1} at the blaze angle with single path ($p=1$) and double path ($p=2$) operations, respectively. The optical layouts are shown in Fig. 3 for a single path operation and in Figs. 4 and 5 for a double path operation. The collimating mirror M11 has a focal length of 2500 mm and a diameter of 300 mm. The f-number of the monochromator is about 25. For the double path operation, the light beam from the entrance slit S1 illuminates the grating G, after being collimated by the mirror M11. The reflected light from G is focused upon the spherical mirror M9 ($R=1000$ mm) at I1. The image at I1 is transformed to I2 by the spherical mirror M10 ($R=500$ mm). After being collimated and reflected by M11 and G once more, the light beam is finally focused upon the exit slit S2 (see Figs. 4 and 5).

Since the light beam is chopped just before the entrance slit S1, the single-pass radiation and the double-pass radiation must be separated optically. If the upper half of the entrance slit is masked, the image at S1 is transferred to the lower half of S2 with respect to the optical axis in the case of double pass operation. For the case of single pass operation, on the other hand, the upper half image at S1 is transferred to the lower half image at S2. Therefore, a double pass component can be definitely separated from a single pass component by masking either upper or lower halves of the entrance and exit slits. The situation is illustrated in Fig. 5, where the dotted line corresponds to the optical axis and the image I1 of double pass operation corresponds to the image S2 of single pass operation. The points at I1 and I2 are conjugated with respect to M10, while the points at S1 and S2 are conjugated with respect to M10. The grating pupil is focused upon the field mirror M10 and, therefore, M10 can be as small as 20×20 mm^2.

The slits S1 and S2 have the heights of 80 mm, but only the lower halves of about 30 mm are used for a double path operation. For the double path operation, both entrance and exit slits[3] have a radius of curvature of 640 mm. For the single path operation, S1 is a straight slit and S2 has a curvature. The curvature of 640 mm is based upon the sagittal curvature calculated at the blaze angle. Although the curvature is slightly different at the other angles, the difference is negligible because relatively small range of angle is used for the actual scanning (see Fig. 1). Moreover, if half of the slit is masked, effect of the different angles becomes much smaller.

The aberration which arises from the use of a spherical mirror for M11 is examined carefully by the beam tracing method using a large electronic computer. A few results are illustrated in Figs. 6a and 6b. In this

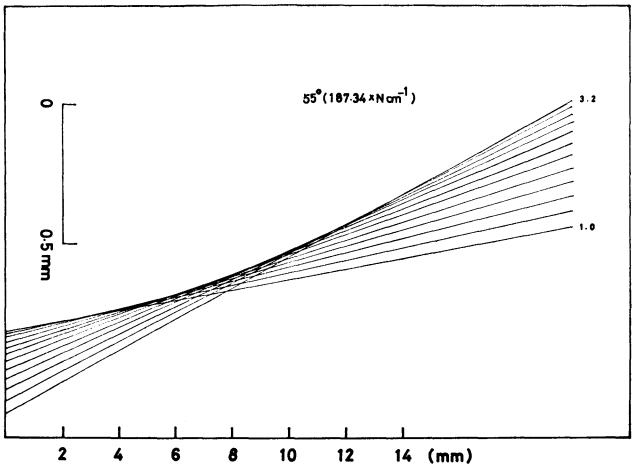

6a. Incident angle to the grating is 55°.

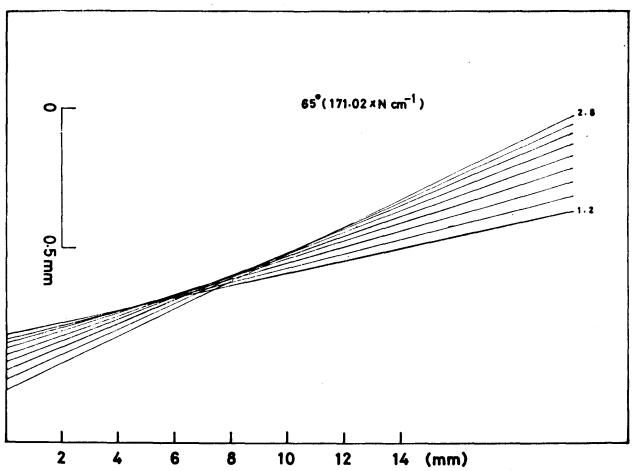

6b. Incident angle to the grating is 65°.

Fig. 6. Results of beam tracing by computer. The entrance slit is put at the origin which is 2500 mm apart from the collimating mirror. Spindle axis parallel to optical axis. Small figures of the right side show angles of the ray at entrance slit. Note that scales of the spindle and cross axes are different.

calculation, the entrance slit is put at the origin which is 2500 mm apart from M11. The diffuseness at the focal point is about 0.06 or 0.04 mm for the incidental angle of 55° or 65°, respectively. Because the mechanical slit width used for the ordinary spectral measurements is 0.4—0.2 mm, the effect of the aberration is negligibly small. Figure 6 shows that the focal point at the exit slit is about 8 mm forward. Therefore, the entrance and exit slits are simultaneously moved about 4 mm forward along the optical axis, because S1 and S2 must be optically conjugated.

Fore-optics and White Cell. For a measurement of high-resolution infrared spectrum, it is necessary to use a long path cell, for the line width due to pressure broadening often exceeds the spectral width of a monochromator even under low sample pressure. Thus, we designed the fore-optics with a long-path cell of White type[4] optically matched to the monochromator.

Figure 7 shows the optical layout of the fore-optics with a White cell. The light from the source S0 is focused by an ellipsoidal mirror M1 at the point very

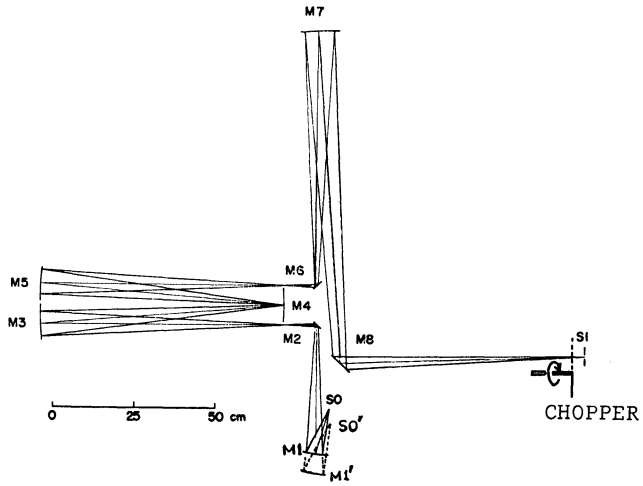

Fig. 7. Optical layout of fore-optics with White cell.

close to the KBr window of the White cell. After being reflected multiple times in the White cell between the spherical mirrors M3, M4, and M5, the light beams are focused on the entrance slit S1. The *f*-number is matched to 25 which is the same with that of the grating monochromator. As the *f*-number at the source S0 is about 3.75, the source image is magnified by about 6.6 at S1. The ellipsoidal mirror M1 and the spherical mirror M7 are used for the *f*-number matching.

The White type long-path cell has three spherical mirrors with a focal length of 757.9 mm and has two KBr windows with diameters of 70 mm. This cell is optically matched with the spectrometer. The light beam is guided into the cell by the plane mirror M2. The White cell has a physical length of about 75 cm between the mirrors M3 and M4, or M5 and M4, giving path length up to 30 m. The sampling system of a vacuum line is always combined with the White cell, which guarantees the vacuum of about 10^{-5} Torr when there is no sample in the system.

The White cell can be removed and mirrors M2 and M6 are used to bring the radiation out to an external sampling device and return it to the vacuum instrument. Mirrors M2 and M6 can be removed, giving a sample space for a short cell use. In this case, it is necessary to translate a mirror M1 and a source S0 to the positions M1′ and S0′. Both components are mounted on a single plate which slides along the rail parallel to the optical axis.

The source S0 is a Nernst glower purchased from Perkin-Elmer with an active length of 20 mm. The source is covered with a brass mantle. The electric circuit involves a 60 W balast lamp. The conditions of the source operation are 0.3—0.45 A and 80—100 V. The stability of the light source is quite satisfactory in the vacuum, because there is no convection of air in the vacuum.

Order Sorter. The optical layout of the order sorter is shown in Fig. 8. The order sorter is essentially a prism spectrometer of Wadsworth mount and separates the order of a grating. The prism P and the Wadsworth mirror M15 are mounted on a single plate and is rotated so as to keep the angle of minimum deviation.

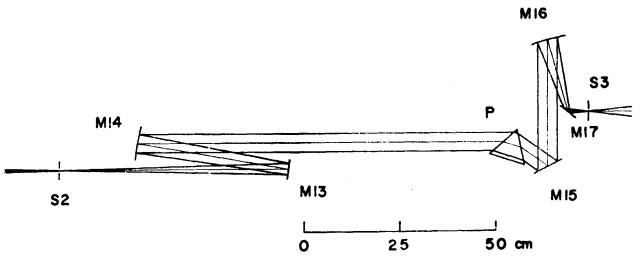

Fig. 8. Optical layout of order sorter.

Three different prisms of KBr, NaCl, and CaF_2 are used for the different frequency ranges. They are 60° prisms with 70 mm in height and with 100 mm base length.

The light beam from the exit slit S2 of the grating monochromator is collimated by the parabolic mirror M14 which has a focal length of 1000 mm. After being separated into grating orders by the prism P, the light beam is focused on the exit slit S3 of the order sorter by the parabolic mirror M16 of a focal length of 250 mm. Therefore, the image at S3 is one fourth of the image at S2. A straight slit is used for S3, because the prism P is oriented so that the curved image at S2 is changed into the straight image at S3. The position of P is at an exit pupil of the grating. The mirror M16 is positioned to give another exit pupil of the grating at about 300 mm behind the exit slit S3.

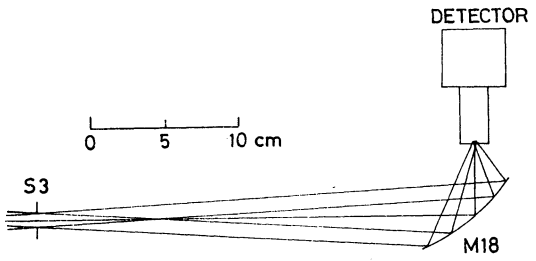

Fig. 9. Optical layout between exit slit and detector (vertical).

In order to collect the radiation to the detector, we used an ellipsoidal mirror M18 by which the light beam is vertically reflected and focused upon the detector element (see Fig. 9). The exit slit S2 is finally imaged upon the detector with a magnification of about one twenty-fourth. The detector is positioned out of the vacuum tank and the distance from the exit window of

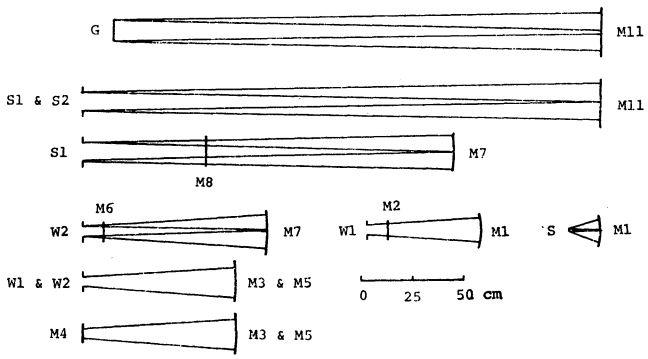

Fig. 10. Vertical tracing for grating monochromator (for single pass) and fore-optics.

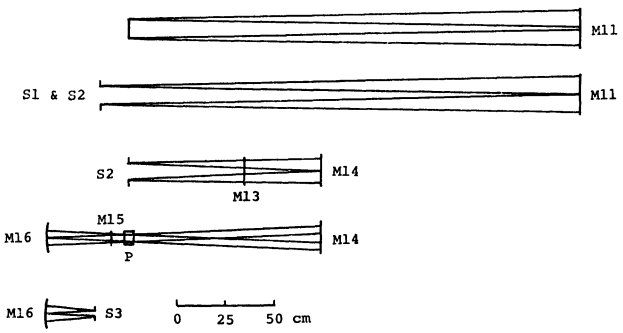

Fig. 11. Vertical tracing for grating monochromator and order sorter.

TABLE 1. DETAILS OF MIRRORS

Name	Type	Dimension (mm)	Remarks
M1	ellipsoidal	150×78	a=325.0, b=269.5, α=22°
M2, M6	plane	80×50	
M3, M5	spherical	160×125	R=757.9
M4	spherical	60×110	R=757.9
M7	spherical	230 ϕ	R=1207.43
M8	plane	150×90	
M9	spherical	55×55	R=1000
M10	spherical	40×40	R=500
M11	spherical	300 ϕ	R=5000
M12	plane	80×25	
M13	plane	180×50	
M14	parabolic	150×80	f=1000, α=6°
M15	plane	100×90	
M16	parabolic	100×70	f=250, α=15°
M17	plane	80×35	
M18	ellipsoidal	80×70	a=175.0, b=86.6, α=19°

R: Radius of spherical mirror (mm), f: focal length of parabolic mirror (mm), a: a half of longer axis of ellipsoidal mirror (mm), b: a half of shorter axis of ellipsoidal mirror (mm), α: off-axis angle.

the vacuum spectrometer to the mirror M18 is about 15 cm. One can use this space to put a short path gas cell for the calibration purpose or the usual spectral measurement.

Mirrors. All the mirrors used are made on BK7 glasses and the thickness is greater than one fifth a diameter. Aliminum surface is coated with silicon monoxide. An accuracy of a surface is better than $\lambda/2$ (λ=546 nm). The dimensions of the mirrors are determined by drawing the plane figures (see Figs. 2, 3, 4, 7, and 8) and the vertical figures (see Figs. 5, 9, 10, and 11) of the optical layout. In Table 1, the mirrors used are summarized with the types and dimensions.

Detection System

The detection system adopted in this spectrometer is a phase sensitive detection system. The schematic diagram of the whole system is shown in Fig. 12. A mechanical chopper of a rotating circle is positioned just in front of the entrance slit S1 and chops the signal and reference signal beams simultaneously. The rotating circle has six wings made of a pasteboard and is jointed to the direct current vacuum motor[6] which rotates

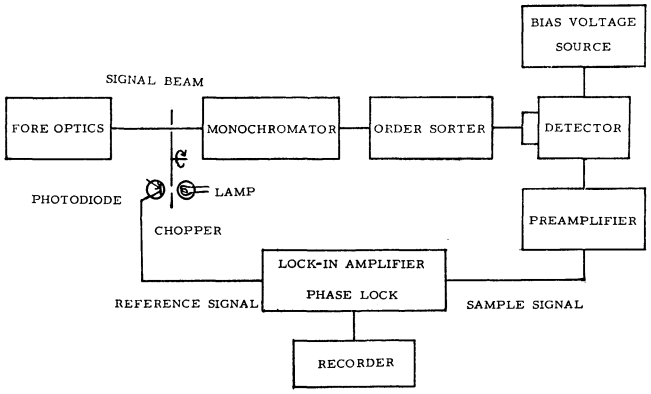

Fig. 12. Detection system (schematic).

about 100 Hz in vacuum. Therefore, the light beams arrive at the detector is a 600 Hz alternating pulse signal. After being amplified by a preamplifier,[7] the signal from the detector is put into the lock-in amplifer[8] and compared with the reference signal. The 6.3 V midget lamp is used as the reference light source and the light energy is transformed into electric current by the phototransistor OS14. The final output from the lock-in amplifier is direct current and is sent to recorder.[9]

Detector and Preamplifier. As an actual resolution of a spectrometer is governed by a signal to noise ratio, detectivity of a detector is the most important problem for the construction of a spectrometer. In our spectrometer, an InSb semiconductor detector is used for the region around 2000 cm^{-1}, a Ge: Au detector below 1800 cm^{-1} region, and a PbS detector above 3000 cm^{-1} region. The detectivity of InSb detector is higher than that of Ge: Au detector about one order of magnitude at 2300 cm^{-1} region. The ν_2 band of carbon dioxide is measured by use of these two different types of detectors under the same instrumental conditions. The S/N ratio of the spectra for InSb detector is about ten times better than that for Ge: Au detector. Although at the longer wavelength region, there are a few detectors which are superior in detectivity to Ge: Au detector, they must be cooled by liquid helium. At the present situation of our laboratory, it is rather inconvenient and troublesome to use liquid helium. Thus we decided to use a Ge: Au detector for the longer wavelength region.

The preamplifiers suitably designed to the individual detectors are made by ourselves. The amplification factors are limited to 20—50 dB.

The InSb detector was purchased from JEOL, Ltd.,[10] with the sensitive area of 1×1 mm^2. The preamplifier and the bias voltage supplier were constructed according to the data sheet, the amplification degree being about 30 dB.

The Ge: Au detector was purchased from Barnes Co.,[11] with the sensitive area of 2×2 mm^2. The magnitudes of bias voltage and load registor are adjusted to the recommended values from the detector manufacturer. The preamplifier was made by the use of an operational amplifier of Burr-Brown model 3503A.[12] The amplification degree is about 50 dB.

The PbS detector was purchased from Infrared Industries[13] with the sensitive area of 2×2 mm^2.

Vacuum System and Room

The elimination of atmospheric carbon dioxide and water vapor is essentially important, because they have strong absorption bands in the infrared regions. Since the optical pathlength of the entire system is about 30 m long, it is desired to build a spectrometer in vacuum.

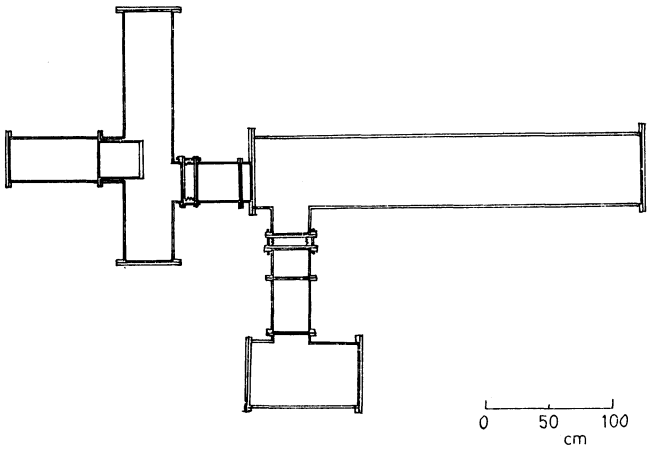

Fig. 13. Vacuum tank.

Figure. 13 shows a plane tracing of a vacuum tank system. The tank system is conveniently separated into three parts in accordance with the optical system, *i.e.*, a main tank, a fore-optics tank, and an order sorter tank. These three parts are connected with each other by bellows flanges which can be collapsed and removed without disturbing the optical system, since there are no internal optical benches inside of the bellows sections. This system is beneficial to avoid the spread of distortions of the individual tank due to temperature changes and to evacuation. All the flanges and end covers are sealed with O-rings. Removing these covers and bellows sections, we can set and adjust all the necessary optical elements effectively.

A rotary pump[15] is used to evacuate the vacuum tank with evacuation speeds of 3000 l/min. As the total volume of the tank is about 1000 l, we can reach pressures of about 10^{-3} torr within a few minutes. Using an oil diffusion pump,[16] we have actually reached pressures of 10^{-4} Torr, although it is not always necessary to operate the spectrometer under such low pressure. In order to avoid the mechanical vibration transferred from the main rotary pump, we can use a supplementary pump of 450 l/min evacuation speed[17] after the spectrometer is evacuated by the main pump.

The detector system is placed out of the vacuum tank and, therefore, nitrogen gas is flashed to remove atmospheric carbon dioxide and water vapour. Actually the detector system is confined in an aluminum box. The disturbing absorption lines of these molecules were reduced to about one twentieth by flashing dry nitrogen gas inside of the box.

In order to avoid the effect of mechanical vibrations of room floors, the spectrometer base is fixed rather loosely to the floor by the use of sand and mortar as illustrated in Fig. 14. In addition, optical benches

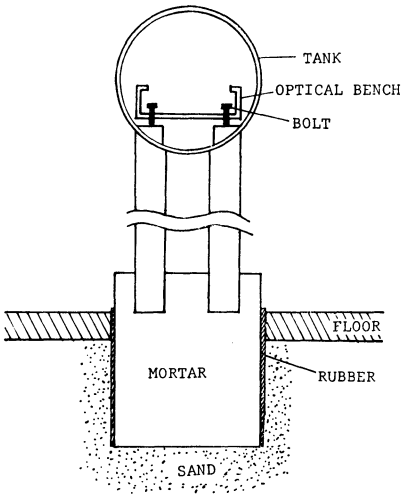

Fig. 14. Schematic figure for spectrometer base. Optical bench is mounted on vacuum tank kinematically.

are kinematically mounted so that the distortion and vibration of the tanks would not directly disturb the optical set-up.

The room is airconditioned,[18] which keeps the temperature and humidity of the room within 23±0.5 °C and 45±5%. The variation of the temperature will cause the thermal expansions of optical benches and vacuum tanks, which will disturb the optical alignment of the spectrometer.

Mechanical System[19]

Driving Mechanism of Grating. The most principal part of all the mechanisms is a driving mechanism of a grating, because it governs an accuracy of frequency measurements. Figure 15 shows the plane figure for the grating drive mechanism. Figure 16 is the cross section of the rotatory shaft of the grating drive. The mechanism is arranged to give both fine and coarse drives. The former is used for the precise measurements under optimum resolution, while the latter is used for the survey works and for setting the instrument to a suitable wavelength range. The coarse driving mechanism is extremely convenient and indispensable for actual measurements.

As shown in Figs. 15 and 16, the rotatory shaft is composed of three coaxial cylinders made of stainless steel. The outer cylinder is fixed to the optical bench. The intermediate cylinder is equipped with a 400 mm tangent arm and rotates inside the outer cylinder. The weight of this cylinder is supported by a ball bearing which is set upon the outer cylinder. Since the cylinder faces are carefully polished, the rotation is very smooth. The tangent arm is pushed by a stainless steel rod which is connected to a 50 mm micrometer head.[20] The micrometer is driven through a gear box external to the vacuum tank. The rotatory rod which connects the micrometer and the gear box is sealed by O-rings as shown in Fig. 17. The gear box is designed to give six scanning speeds from about $(5n/2)$ to $(5n/64)$ cm^{-1}/h, where n is the grating order.

The inner cylinder, upon which the grating is mounted, is rotated by a worm and wheel of about 160 mm diameter. This part is placed upon the tangent arm and is designed for coarse driving purpose. The inner cylinder is driven by a second gear box which is set out of the vacuum tank. Scanning speed is changeable from $20n$ to $640n$ cm^{-1}/h, where n is the grating order. The diameters of these three cylinders are 120, 80, and 40 mm.

In order to determine the frequencies with the

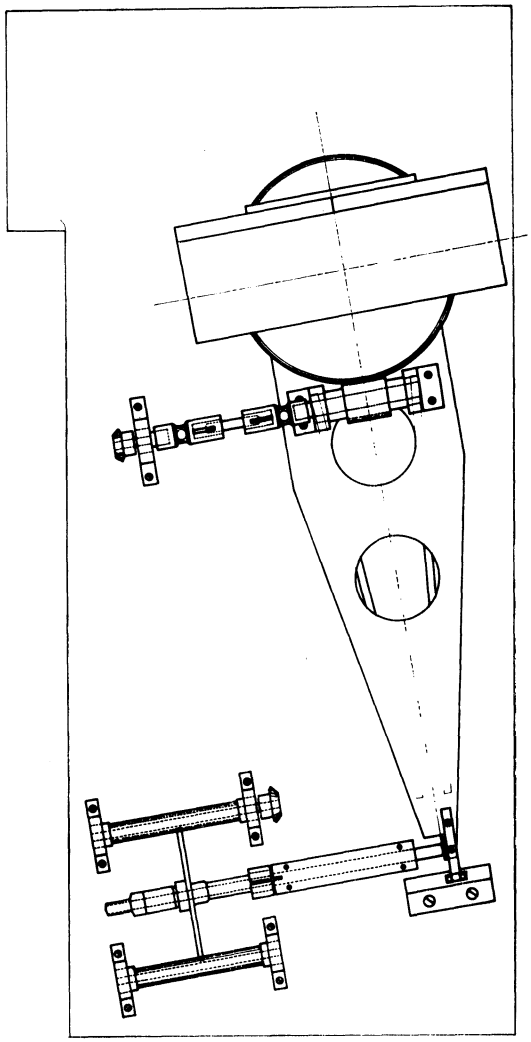

Fig. 15. Plane figure of grating drive mechanism.

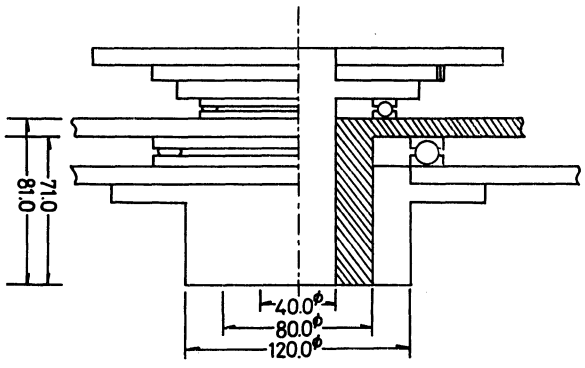

Fig. 16. Cross section of rotating shaft of grating drive mechanism.

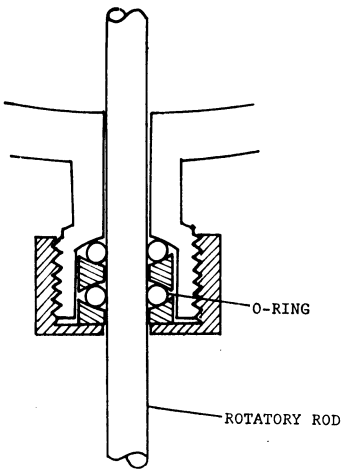

Fig. 17. Sealing of rotatory rod.

accuracy of 0.002 cm^{-1}, the grating must be rotated with the accuracy of 1 second of arc. As mentioned above, the fine drive mechanism consists of a 400 mm tangent arm and a 50 mm micrometer head. The required accuracy can be satisfied, because the accuracy of the micrometer drive is ascertained to be better than 0.01 mm.

Driving Mechanism of Prism. The prism drive mechanism is essentially the same as that of grating drive. A bearing of 30 mm diameter is connected to the nut which, in turn, slides along the screw. We manually drive the screw from outside the vacuum tank. No provision is made for coupling the prism rotation with that of the grating mechanically, because the setting of prism rotation must be changed only about once an hour under normal running conditions.

Mirror Holders. Modified Perkin-Elmer mount has been applied for the design of all the mirror holders, except for the spherical mirrors, M7 and M11. The holders for M7 and M11 can slide along a guiding rod by a screw and a nut which is fixed to the mirror mount (see Fig. 28). We can accurately adjust the position of the mirror by driving the screw.

Performance

As mentioned earlier, a particular order of an echelle type grating has a narrow frequency region. Using a few orders, however, we can cover the wider frequency region (see Fig. 1). Firstly we have to know the relation between the grating order and the rotating angle of a prism. The grating is fixed at a particular position and the prism is rotated slowly by hand. As shown in Fig. 18, we can observe the successive intensity maxima along the angle of prism rotation. The grating order can be determined from the cut off frequency of the detector and the atmospheric CO_2 absorption. The 4.5 μ absorption band of carbon dioxide is observed in the 13-th order.

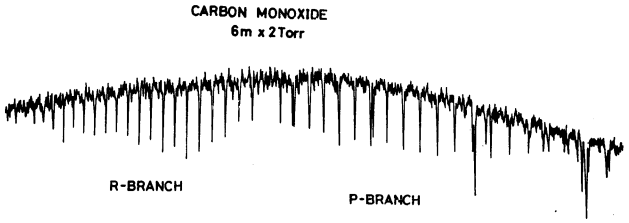

Fig. 19. Rapidly scanned spectra for CO.

Next procedure is to determine the relation between the coarse drive counter and the frequency. The carbon monoxide has absorption lines in fairly wide region with regular spacing. Fixing the prism angle at 12-th order of the grating, we scan the coarse driving mechanism without moving the fine drive. We obtain the CO spectrum as shown in Fig. 19. As the frequencies of CO lines are accurately known,[21] the calibration diagram for the coarse drive can be obtained.

It is necessary to know the relation between the mechanical slit width and the counter number of slit drive mechanism. The entrance slit S1 is fixed about 4 mm wide, and the width of exit slit S2 is changed from 2.00 mm to zero. Since the energy which reaches at the detector is proportional to the width of S2, we can calibrate the mechanical slit width against the counter number of the slit S2. The same method is applied to the entrance slit S1.

The resolving power of the spectrometer is checked by observing the ν_3 band of NNO, $2\nu_3$ band of CH_3F, 10 μm CO_2 laser lines and so on. The line width of CO_2 laser line is about 0.002 cm^{-1} for the multimode operation, which corresponds to a Doppler breadth. Since the diffraction limit of the grating of this spectrometer is about 0.027 cm^{-1} for single pass operation, the line width of the CO_2 laser is negligibly small. In Fig. 20 shows the observed spectrum of CO_2 laser

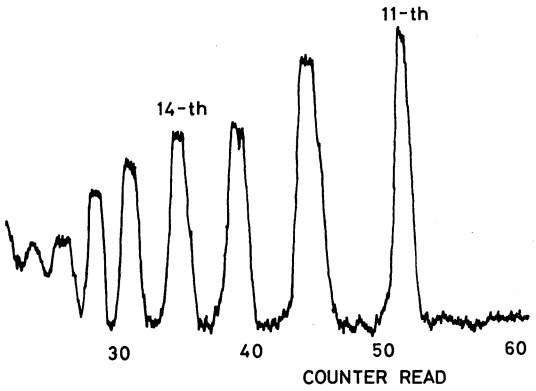

Fig. 18. Grating orders and prism counter.

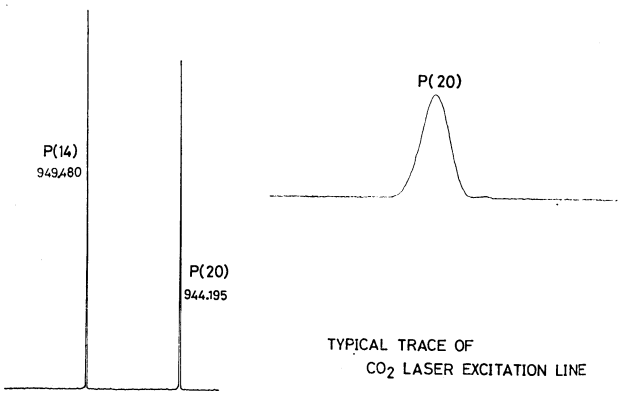

Fig. 20. Typical trace of CO_2 laser line.

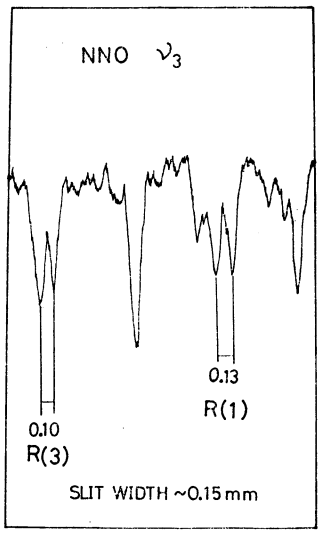

Fig. 21. Resolution check by ν_3 band of NNO. Single pass operation, InSb detector.

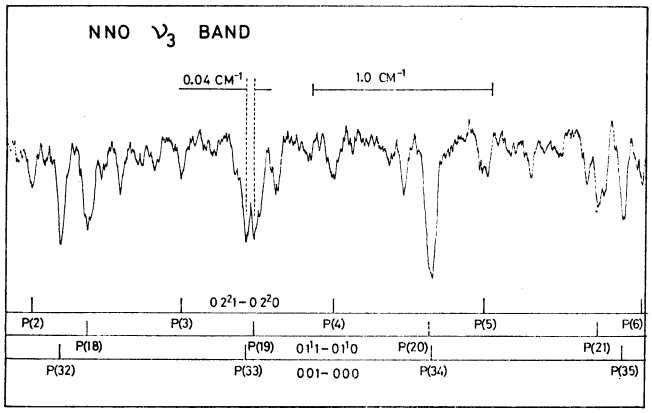

Fig. 22. Resolution check by ν_3 band of NNO. Double pass operation, InSb detector.

line. The half width of the observed line is about 0.03 cm^{-1}, which corresponds to the resolution limit for the single pass operation.

For usual measurements, the resolution is limited by a signal to noise ratio which is governed by the detectivity of a detector. As the ν_3 band of NNO has a number of hot band series, the absorption lines have various separation. Figure 28 shows the observed spectra of the ν_3 band of NNO with a single pass operation using an InSb detector. The resolution is better than 0.07 cm^{-1}, although this region is far from the blaze angle of the grating. In Fig. 22, the spectra of ν_3 band of NNO observed with a double pass operation is shown with their assignments. These lines are seen to be measured with good S/N ratio and the resolution is ascertained to be better than 0.04 cm^{-1}.

The ^qQ-branch of $2\nu_3$ band of CH_3F is completely resolved into its J-components and the individual J-component is resolved into a lot of K-components. From the spacing of the resolved lines, the resolution is ascertained to be better than 0.04 cm^{-1}. The detailed analysis of the band has been given in elsewhere.[22]

An accuracy of a frequency measurement is estimated from the standard deviation of the CO calibration lines fitted with the quartic equation. The standard deviation of the actually observed CO lines is about 0.005 cm^{-1}. The value of 0.005 is obtained from a single measurement and the error arises mainly from the reading ambiguity of the line positions.

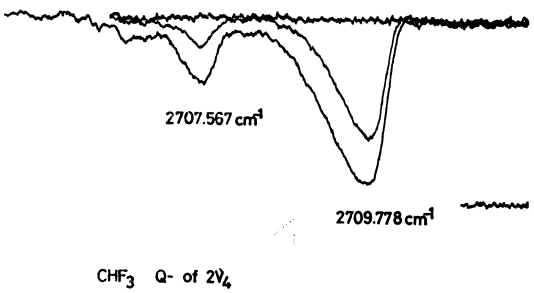

Fig. 23. Q branch of $2\nu_4$ and related hot bands of CHF_3.

The intensity accuracy is checked by observing relative intensities of the Q branch of the $2\nu_3$ band of CHF_3, the observed result of which is shown in Fig. 23. The three Q branches are assigned to one main band and two hot bands. As the intensity of the Q branch is proportional to the Boltzmann factor, we can ascertain the accuracy of the intensity measurements by comparing the theoretical and observed intensity ratios of the three Q branches. The result indicates that the accuracy along an intensity axis is better than $\pm 3\%$ of the full-scale disregarding to the effect of the S/N ratio.

Photographs of the Spectrometer

Photographs of the spectrometer are summarized in Figs. 24—29. In Fig. 24 a part of the monochromator tank is seen at the right hand side and the order sorter tank at the lower left. These two tanks are combined with bellows flanges. The fore-optics tank is seen at the middle of the picture. The vacuum lines which is seen at the upper side is the sampling system. Figure 25 shows the fore-optics with a long path cell of White type. Behind the fore-optics tank, the flange of the monochromator is seen. The U-pipe leads to the vacuum pump. Figure 26 shows the top view of the grating monochromator. The grating and the coarse driving mechanism are clearly seen. At the upper left we see the entrance slit S1 and double pass mirror M9.

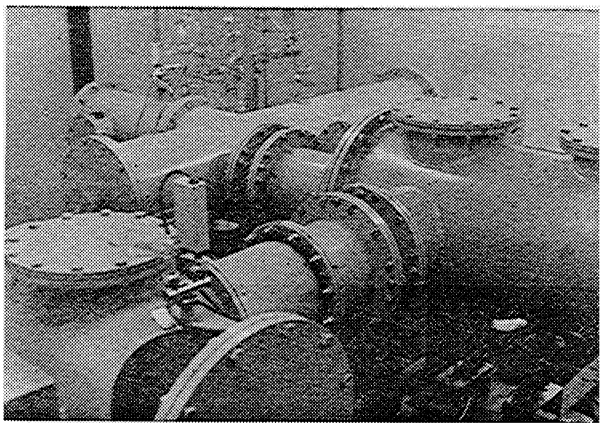

Fig. 24. Vacuum tank (whole view).

Fig. 25. Sampling system.

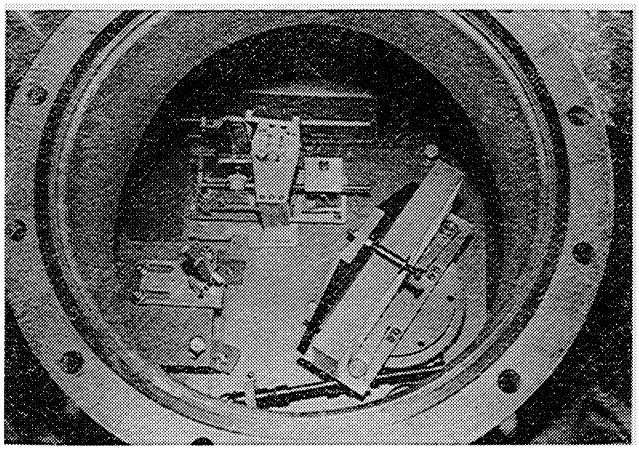

Fig. 26. Top view of grating monochromator.

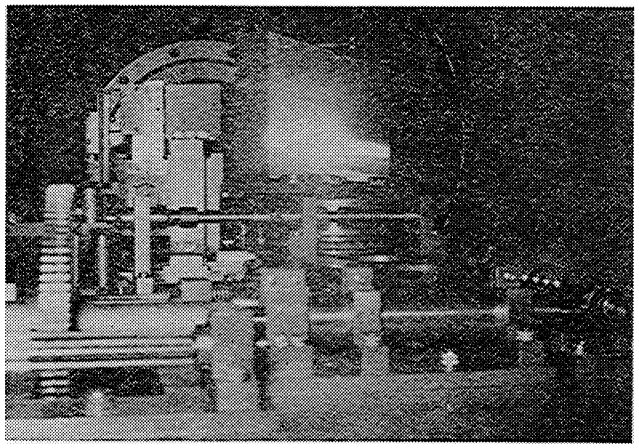

Fig. 27. Side view of grating monochromator.

The coarse driving mechanism consists of a worm and wheel. The side view of this part seen from the direction of the collimator mirror is shown in Fig. 27. The grating strongly reflects the flash-lamp light. Behind the grating, the entrance slit and double pass mirror M9 are seen. The fine drive mechanism which consists of the micrometer and the tangent arm is seen before the grating. In Fig. 28, we can see the optical bench and the mirror holder inside the main tank. Note that the optical bench is supported by bolts and is not fixed to the tank directly. The order sorter part is

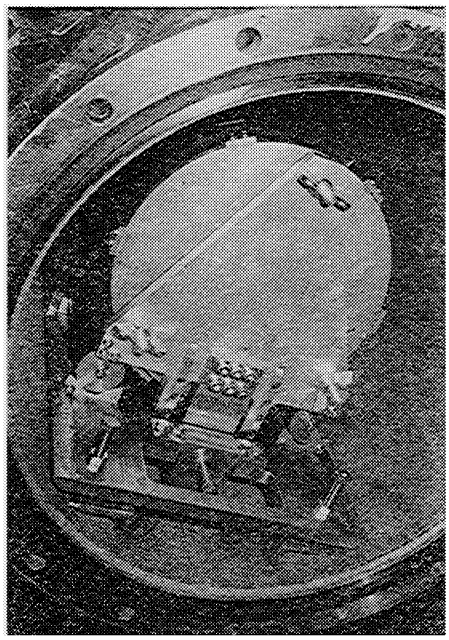

Fig. 28. Collimating mirror.

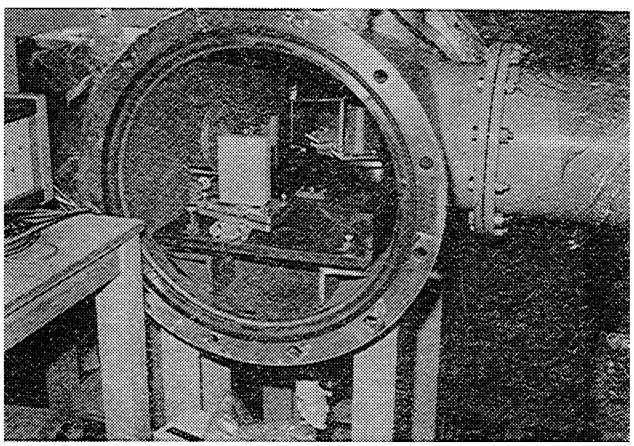

Fig. 29. Order sorter.

seen in Fig. 29. The prism and M15 are placed on the same rotatory holder.

References

1) J. Connes, and P. Connes, *J. Opt. Soc. Am.*, **56**, 896 (1966); P. Jacquinot, *Appl. Opt.*, **8**, 497 (1969); J. Connes, H. Delonis, P. Connes, G. Guelachuili, J. P. Maillard, and G. Michel, *Nouv. Rev. Optique Appliquee*, **1**, 3 (1970).

2) J. Overend, A. C. Gilby, J. W. Russel, C. W. Brown, J. Beutel, C. W. Bjork, and H. G. Paulat, *Appl. Opt.*, **6**, 475 (1967); see also T. K. McCubbin, Jr., R. P. Grosso, and J. D. Mangus, *Appl. Opt.*, **1**, 431 (1962); T. K. McCubbin, Jr., J. A. Lowenthal, and H. R. Gordon, *Appl. Opt.*, **4**, 711 (1965).

3) J. U. White, *J. Opt. Soc. Am.*, **32**, 285 (1942).

4) The slit jaws were made of flat stainless steel by ourselves. After roughly making the shape of slit jaws, we accomplished the jaw to a final shape by an oilstone and oil.

5) Mizojiri Kogaku Kogyosho, Tokyo, Japan.

6) Olympus Precision Co., Ltd., Tokyo, Japan, Model CL-4B, 24V, 2.2W.

7) We made a preamplifier to match the detector.

8) NF Circuit Design Block Co., Ltd., Tokyo, Japan, Model LI-572B.
9) Hitachi Co., Ltd., Tokyo, Japan, Model 1001.
10) JEOL, Ltd., Tokyo, Japan, Model 101S and 501S.
11) Barns Engineering Company, Connecticut, USA, Model A-200 series.
12) Burr-Brown Research Corporation, Arizona, USA, Model 3503A.
13) Infrared Industries, Inc., Mass., USA, Type B3 with a liquid nitrogen 4-hour hold Dewar.
14) Sanwa Ulvac Co., Ltd., Tokyo, Japan.
15) Nihon Shinku Co., Ltd., Tokyo, Japan.
16) Nihon Shinku Co., Ltd., Tokyo, Japan.
17) Nihon Shinku Co., Ltd., Tokyo, Japan.
18) Ohnishi Netsugaku Co., Ltd., Tokyo, Japan.
19) The design of all the mechanisms is performed by ourselves. The construction is done by Shotoku Mfg. Co., Ltd., Kawasaki, Japan.
20) Mitsutoyo Mfg. Co., Ltd., Tokyo, Japan, Model 151-256, MHHl-50.
21) K. N. Rao, C. J. Humphreys, and D. H. Rank, "Wavelength Standard in the Infrared," Academic Press, New York (1966).
22) J. Nakagawa, I. Suzuki, T. Shimanouchi, and T. Fujiyama, This Bulletin **46**, 3399 (1973).